Self-Curing Decoupling Technique for Two Inverted-F Antennas With Capacitive Loads

Jiangwei Sui, *Student Member, IEEE*, and Ke-Li Wu, *Fellow, IEEE*

***Abstract*— A new concept named the self-curing decoupling technique is proposed for the first time to reduce the mutual coupling between two closely located inverted-F antennas (IFAs). The decoupling technique only requires a capacitive load on the shorting arm of each coupled IFA without connecting a circuitry or inserting a physical structure between the two coupled antennas. The capacitive load occupies very little space and is frequency-insensitive; therefore, the decoupling technique is a very favorable choice for low-frequency applications. Network analysis is presented to mathematically justify the working mechanism and to provide a design guideline. Several practical cases of two IFAs situated at different positions on the periphery of a PCB board are studied. The experimental results show that with the decoupling technique, significant improvements in the port isolation (from 10 to 20 dB), antenna correlation coefficient (from 0.25 to 0.05), multiplexing efficiency (from 46% to 60%), and above all the system throughput (1.2 and 0.8 dB power saving in Urban Microcell and Urban Macrocell channels, respectively) can be obtained.**

***Index Terms*— Antenna array, decoupling technique, inverted-F antenna (IFA), long-term evolution (LTE), multiple input multiple output (MIMO), mutual coupling, throughput test.**

I. Introduction

TO SATISFY the fast increasing demand for higher data rate and better quality of service, multiple-antenna techniques are widely used in today's wireless communication systems. There are mainly two types of multiple-antenna schemes: *spatial diversity* that enhances the performance of signal throughput by improving the reliability of a system against various channel fading and *spatial multiplexing* that improves the channel capacity by utilizing multiple uncorrelated signal paths. The former is called diversity antenna and the latter is referred to as multiple input multiple output (MIMO) antenna. The MIMO technology has become a paramount means nowadays in wireless communications, from base stations to smart phones and Wi-Fi modules. For multiple antennas in a mobile terminal, an inverted-F antenna (IFA) would be a competitive choice due to its low profile, compact size, design simplicity, and many straightforward multiband options. Nevertheless, due to a limited space in a mobile terminal and the needs for coexistence of multiple antennas for different communication systems, severe mutual coupling and high spatial correlation among the antennas will diminish the benefits to channel capacity and diversity gain of the antenna system [1]. In addition, strong coupling also lowers the total efficiency of the antenna system as the coupled antenna acts as a load that dissipates the energy. Moreover, high isolation between transmitting and receiving antenna ports is crucial for an in-band full-duplex communication system, which has a large potential to be adopted in future wireless systems [2].

Tremendous research efforts have been devoted to the performance improvement of a multiple-IFA MIMO system for wireless terminals. In [3], several multiple-IFA antenna configurations for mobile handsets are investigated with respect to their mutual coupling. The results show that the relative position of the antennas may be optimized to obtain low mutual coupling and a low envelope correlation coefficient (ECC) between the antenna elements. The relative position of the feeding and shorting points of IFA antennas could also be optimized to achieve a good MIMO antenna performance [4].

Many decoupling techniques have been proposed in the community to mitigate the mutual coupling between antennas. The space, polarization, and angle diversity between antennas can be directly utilized to reduce mutual coupling [5]. Such approaches are straightforward to implement if space permits, especially at high frequencies. A neutralization line can be used to connect two coupled antennas to neutralize the mutual admittance [6], [7]. Inserting a parasitic (or dummy) element between antennas is also a common technique to achieve good isolation [8]–[10]. A special ground structure or electromagnetic band-gap structure can be introduced between antennas to reduce mutual coupling by manipulating the surface wave or the current flowing between antennas [11]–[15]. A transmission line circuit [16], [17], an *LC* circuit [18], [19], a coupler [20]–[22], or a coupled resonator circuit [23]–[25] can be connected between coupled antennas to mitigate mutual coupling. Generally speaking, the dimensions of above-mentioned structures or circuits are in the order of half a wavelength. In addition, one need to find sufficient space to lay the connecting transmission lines between antennas, which is not a convenient practice as a wireless terminal is usually densely populated by electronic components.

In this paper, a simple but an effective decoupling technique for two IFA antennas is proposed. The technique introduces

Manuscript received August 18, 2017; revised November 14, 2017; accepted December 26, 2017. Date of publication January 5, 2018; date of current version March 1, 2018. This work was supported by the Postgraduate Scholarship of The Chinese University of Hong Kong. *(Corresponding author: Ke-Li Wu.)*

The authors are with the Department of Electronic Engineering, The Chinese University of Hong Kong, Hong Kong (e-mail: jwsui@ee.cuhk.edu.hk; klwu@ee.cuhk.edu.hk).

Color versions of one or more of the figures in this paper are available online at http://ieeexplore.ieee.org.

Digital Object Identifier 10.1109/TAP.2018.2790041

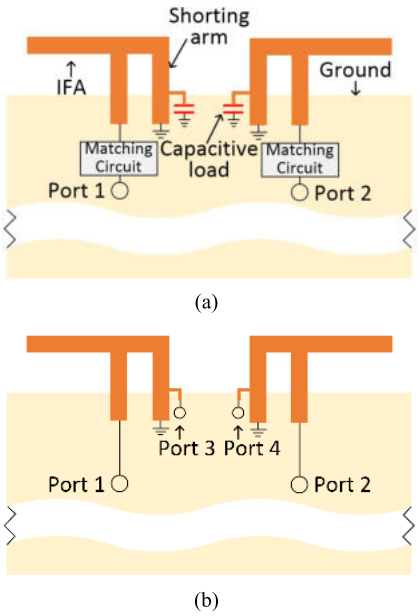

Fig. 1. (a) Proposed decoupling scheme for two IFA antennas. (b) Port definition without loads at ports 3 and 4.

a capacitive load at a proper tapping position on the shorting arm of each IFA antenna. Compared with the existing decoupling techniques, the proposed new method has following three unique and attractive features.

1) *Convenience:* Only a capacitive load on the shorting arm of each IFA antenna is needed without introducing a circuit or a structure that physically connects or locates between the two coupled antennas, such as a neutralization line or a decoupling circuit.
2) *Compactness:* The capacitive load occupies very little space and is frequency-insensitive therefore the technique is a very favorable choice for low-frequency applications.
3) *Frequency Selectivity:* One capacitive load only affects the antenna characteristics in a designated frequency band, and multiple-band decoupling can be easily implemented.

This paper is organized as follows. Section II introduces the network analysis and design procedure. Section III shows several proof-of-concept examples targeted to various practical applications. Finally, conclusions and future works are given in Section IV.

II. Network Analysis and Design Procedure

A. Network Analysis

Fig. 1(a) shows the schematic of the proposed decoupling technique, in which a capacitive load is added at a proper tapping position on the shorting arm of each IFA antenna and a matching circuit may be needed at each antenna. To understand the decoupling mechanism and to develop an analytical formula to find the load, a pair of coupled IFAs is treated as a four-port device that can be described by a four-port network as shown in Fig. 1(b), in which ports 1 and 2 are the original feeding ports and ports 3 and 4 are auxiliary ports.

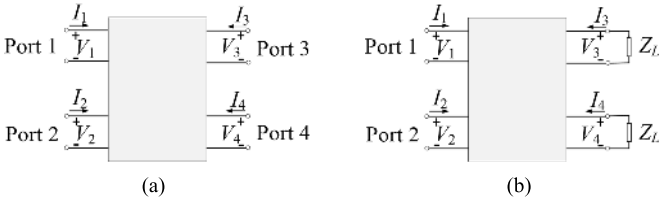

Fig. 2. (a) Four-port network. (b) Two-port network with loads Z_L at ports 3 and 4.

With the port voltages and currents defined in Fig. 2(a), the four-port network can be expressed by its impedance matrix as

$$\begin{bmatrix} V_1 \\ V_2 \\ V_3 \\ V_4 \end{bmatrix} = \begin{bmatrix} Z_{11} & Z_{12} & Z_{13} & Z_{14} \\ Z_{21} & Z_{22} & Z_{23} & Z_{24} \\ Z_{31} & Z_{32} & Z_{33} & Z_{34} \\ Z_{41} & Z_{42} & Z_{43} & Z_{44} \end{bmatrix} \cdot \begin{bmatrix} I_1 \\ I_2 \\ I_3 \\ I_4 \end{bmatrix}. \tag{1}$$

Although the decoupling technique works for both symmetric and asymmetrical cases, for the sake of simplicity, it is assumed that ports 3 and 4 are terminated with the same complex load Z_L as shown in Fig. 2(b), for which the voltage–current relation of ports 1 and 2 becomes

$$\begin{bmatrix} V_1 \\ V_2 \end{bmatrix} = \begin{bmatrix} \overline{Z_{11}} & \overline{Z_{12}} \\ \overline{Z_{21}} & \overline{Z_{22}} \end{bmatrix} \cdot \begin{bmatrix} I_1 \\ I_2 \end{bmatrix} \tag{2}$$

where the values of $\overline{Z_{21}}$, $\overline{Z_{11}}$, and $\overline{Z_{22}}$ are given in (3a)–(3c), respectively, as shown at the bottom of this page.

Equation (3a) shows that the mutual impedance $\overline{Z_{21}}$ of the two-port network can be minimized by properly choosing the network parameters Z_{13}, Z_{23}, Z_{44}, Z_{34}, Z_{14}, Z_{24}, and Z_{33} and the load Z_L. For a given pair of IFAs, changing the tapping position will change the network parameters Z_{13},Z_{23}, Z_{44}, Z_{34}, Z_{14}, Z_{24}, and Z_{33}. As for the load Z_L, it should be reactive with a small but positive real part in order to avoid unwanted loss. Nevertheless, the load will inevitably introduce a small resistance in a practical implementation.

B. Design Formula

Enforcing the decoupling condition by setting $\bar{Z}_{21} = 0$ in (3a), a quadratic equation of unknown Z_L results in two

$$\overline{Z_{21}} = Z_{21} - \frac{Z_{13}Z_{23}(Z_{44}+Z_L) - Z_{34}(Z_{23}Z_{14}+Z_{13}Z_{24}) + Z_{14}Z_{24}(Z_{33}+Z_L)}{(Z_{33}+Z_L)(Z_{44}+Z_L) - Z_{34}^2} \tag{3a}$$

$$\overline{Z_{11}} = Z_{11} - \frac{Z_{13}^2(Z_{44}+Z_L) - 2Z_{13}Z_{14}Z_{34} + Z_{14}^2(Z_{33}+Z_L)}{(Z_{33}+Z_L)(Z_{44}+Z_L) - Z_{34}^2} \tag{3b}$$

$$\overline{Z_{22}} = Z_{22} - \frac{Z_{23}^2(Z_{44}+Z_L) - 2Z_{23}Z_{24}Z_{34} + Z_{24}^2(Z_{33}+Z_L)}{(Z_{33}+Z_L)(Z_{44}+Z_L) - Z_{34}^2} \tag{3c}$$

possible solutions: Z_{L1} and Z_{L2}, as given in (4) shown at the bottom of this page. It is known from physical intuition that the decoupling condition can be practically realized if one of the solutions comes with a positive but close to zero real part. For the IFAs cases studied in the following, it will be found that the solution is always capacitive.

To implement the capacitive load, it is important to introduce a short high-impedance stub at the tapping position. There are two functions for the stub: 1) to find the best possible solution of the load by adjusting its position on the shorting arm and 2) to provide an additional tuning variable of the imaginary part of the load by adjusting its dimension. Multiple options for the stub exist and one can always choose a suitable one for a specific application.

The decoupling method is called self-curing decoupling technique as there is no any circuitry or structure connecting the two coupled antennas, directly or indirectly. The tapping position resembles an acupoint in a traditional Chinese acupuncture therapeutic process for curing a discomfort, an analogy of unwanted mutual coupling.

With $\bar{Z}_{21}$ enforced to zero, according to (3b) and (3c), the original matching condition of each antenna is also changed. Because two antennas have been decoupled, the matching circuits of the two antennas can be retuned independently.

III. Demonstration Cases

To demonstrate the decoupling technique and to elaborate the design procedure, eight cases of combinations of two IFA antennas with different positions and orientations on the periphery of an FR4 PCB board are investigated. The size of the PCB board is 100 mm × 65 mm × 1.6 mm for cases 1 and 3–6, 135 mm × 75 mm × 1.6 mm for case 2 and 70 mm × 55 mm × 1.6 mm for cases 7 and 8. Cases 1–6 imitate a mobile phone and cases 7 and 8 imitate a mobile router. In the EM simulation, the dielectric constant and the loss tangent of the FR4 substrate are set to 4.3 and 0.02, respectively, and the thickness and the conductivity of the copper sheet are set to 35 μm and 3.4×10^7 S/m, respectively. Cases 1 and 2 are simulated, fabricated, and measured to verify the concept of this decoupling technique. The remaining cases are investigated through EM simulation using HFSS. The dimensional parameters for all the cases are illustrated in Fig. 3 and the values are listed in Table I. In cases 1–4, L-shaped stubs are adopted while short-tail stubs are adopted for cases 5–8. For all the eight cases, significant improvements in antenna isolation can be observed after decoupling. In Case 2, a dual antenna long- term evolution (LTE) module is connected with two IFA antennas, and the system performance is experimentally investigated in a multiprobe multipath channel emulator. The measurement results show a significant improvement in throughput.

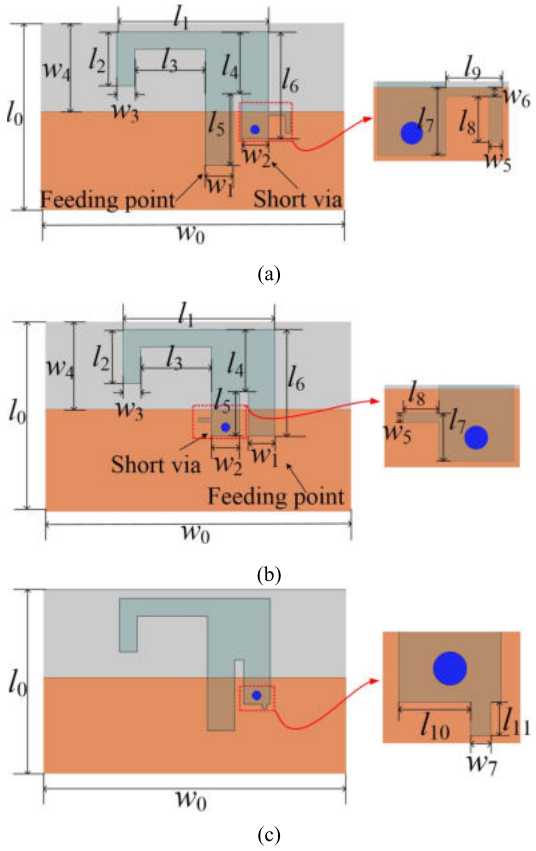

Fig. 3. Dimensions of an IFA antenna with (a) L-shaped load stub for cases 1–4, (b) short-tail load stub for cases 5 and 6, and (c) short-tail load stub for cases 7 and 8. The blue dots denote the short vias.

A. Case 1 (Two Tail-to-Tail IFAs on the Same Edge in ISM Band)

The configuration of two IFA antennas on the same edge of the PCB board working in the 2.45-GHz ISM band is shown in Fig. 4. Although there is no limitation imposed on the symmetry of two IFA antennas, two identical IFA antennas are used for the sake of simplicity. The edge-to-edge distance between the two IFA antennas is 9 mm ($0.0735\lambda_0$).

As discussed earlier, the design of the decoupling circuit involves the following three steps.

Step 1 (Adding a Stub at a Proper Tapping Position on the Shorting Arm of Each Antenna and Introducing Two Auxiliary Ports at the End of the Stubs): Fig. 3(a) illustrates

$$Z_{L1} = \frac{Z_{13}Z_{23}+Z_{14}Z_{24}-(Z_{33}+Z_{44})Z_{21}+\sqrt{[Z_{13}Z_{23}+Z_{14}Z_{24}-(Z_{33}+Z_{44})Z_{21}]^2+4Z_{21}\left[Z_{21}(Z_{34}^2-Z_{33}Z_{44})-Z_{34}(Z_{23}Z_{14}+Z_{13}Z_{24})+Z_{13}Z_{23}Z_{44}+Z_{14}Z_{24}Z_{33}\right]}}{2Z_{21}} \tag{4a}$$

$$Z_{L2} = \frac{Z_{13}Z_{23}+Z_{14}Z_{24}-(Z_{33}+Z_{44})Z_{21}-\sqrt{[Z_{13}Z_{23}+Z_{14}Z_{24}-(Z_{33}+Z_{44})Z_{21}]^2+4Z_{21}\left[Z_{21}(Z_{34}^2-Z_{33}Z_{44})-Z_{34}(Z_{23}Z_{14}+Z_{13}Z_{24})+Z_{13}Z_{23}Z_{44}+Z_{14}Z_{24}Z_{33}\right]}}{2Z_{21}} \tag{4b}$$

TABLE I
PARAMETER VALUES FOR DIFFERENT CASES (UNIT: mm)

	Case	1	2	3	4	5	6	7	8
A1	w_1	3.1	3.1	3.1	3.1	3.1	3.1	3.1	3.1
	w_2	3	3	3	3	3	3	3	3
	w_3	2	2	2	2	2	2	2	2
	w_4	10	10	6	6	6	8	7	7
	w_5	0.6	1.6	0.4	0.4	0.3	0.3		
	w_6	0.4	0.6	0.3	0.3				
	w_7							0.6	0.6
	l_1	17.1	22.1	17.1	19.1	20.7	18.1	18.9	18.9
	l_2	6.1	8.5	5	4	4	7.4	4.3	4.3
	l_3	8	13	8	10	11.6	8	9.8	9.8
	l_4	7	8.5	5	7	6	7	7	7
	l_5	8	0.5	5	5	4	7	5	5
	l_6	12	9	8	10	10	14	10	10
	l_7	3	3	2.5	6	1.5	2.2		
	l_8	2	1.69	2.7	2	2	2		
	l_9	2.51	2.51	2	2				
	l_{10}							1.5	2.1
	l_{11}							0.3	0.6
A2	w_1	3.1	3.1	3.1	3.1	3.1	3.1	3.1	3.1
	w_2	3	3	3	3	3	3	3	3
	w_3	2	2	2	2	2	2	2	2
	w_4	10	10	6	6	6	8	7	7
	w_5	0.6	1.6	0.4	0.4	0.3	0.3		
	w_6	0.4	0.6	0.3	0.3				
	w_7							0.6	0.6
	l_1	17.1	22.1	18.6	17.8	20.4	18.1	18.9	18.9
	l_2	6.1	8.5	4	5	5	7.4	4.3	4.5
	l_3	8	13	9.5	8.7	10.8	8	9.8	9.8
	l_4	7	8.5	7	5	2.4	7	7	7
	l_5	8	0.5	5	5	5.6	7	5	5
	l_6	12	9	10	8	8	14	10	10
	l_7	3	3	1	3	1.2	2.2		
	l_8	2	1.69	1.5	2.7	2	2		
	l_9	2.51	2.51	2	2				
	l_{10}							1.5	2.1
	l_{11}							0.3	0.6

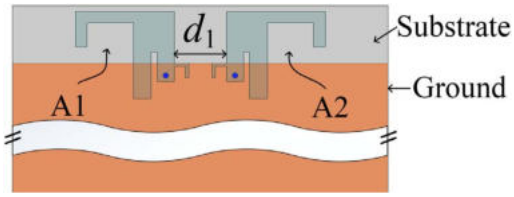

Fig. 4. Configuration of two tail-to-tail IFA antennas for Case 1. The parameter d_1 denotes the distance between antennas. The dots denote the grounding vias.

the dimensions of the IFA antenna. By changing the tapping position of the stubs, an appropriate solution of Z_L can be obtained. Specifically, with $l_8 = 2$ mm, $l_9 = 2.51$ mm, $w_5 = 0.6$ mm, and $w_6 = 0.4$ mm, the solutions Z_{L1} and Z_{L2} versus tapping position parameter l_7 at 2.45 GHz are plotted in Fig. 5. It is observed that the real part of Z_{L1} is close to 0 for a wide range of tapping position l_7, while the imaginary part is always capacitive. In practice, the solution with its real part of about 0.6 Ω can achieve a better decoupling effect than that with 0 Ω because the RF capacitors used in this paper possess about 0.6-Ω inherent resistance. Intensive EM simulation reveals that varying other dimensional parameters of the stub will also lead to a solution with a proper positive

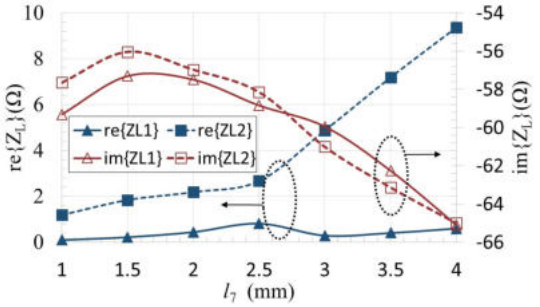

Fig. 5. Load solutions Z_{L1} and Z_{L2} versus tapping position l_7 in Case 1.

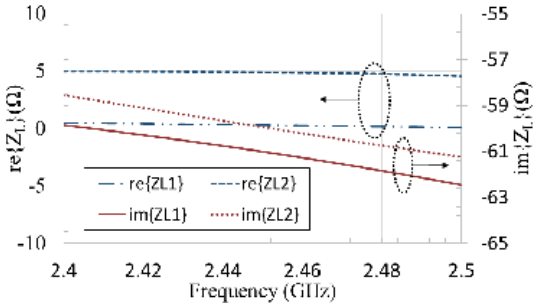

Fig. 6. Load solutions Z_{L1} and Z_{L2} versus frequency in Case 1 with stub dimensions $l_7 = 3$ mm, $l_8 = 2$ mm, $l_9 = 2.51$ mm, $w_5 = 0.6$ mm, and $w_6 = 0.4$ mm.

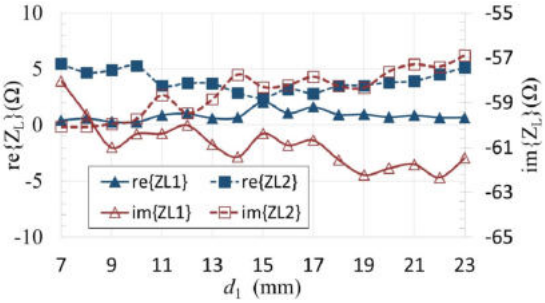

Fig. 7. Load solutions Z_{L1} and Z_{L2} versus distance d_1 in Case 1.

small real part. To further study this case, two solutions with $l_7 = 3$ mm are also calculated in the frequency band from 2.4 to 2.5 GHz as shown in Fig. 6. It is seen that the real part of Z_{L1} is close to 0 over a wide frequency range and the imaginary part is always capacitive. As shown in Fig. 7, the distance d_1 between antenna elements is parametrically studied. It is shown that the real part of Z_{L1} is close to 0 for all the distance studied and the imaginary part is always capacitive.

Step 2 (Adding the Capacitive Loads at the Auxiliary Ports): Both lumped and distributed capacitive loads can be used depending on the convenience in implementation. It can be read from Fig. 6 that the imaginary part of Z_{L1} at 2.45 GHz is about -61 Ω. The parasitic effect of the shorting via is taken into consideration in the field and circuit cosimulation. In this case, two lumped element 0.9-pF capacitors are added at ports 3 and 4.

Step 3 (Rematching the Decoupled IFA Antennas): After adding two capacitors, the original matched condition of each

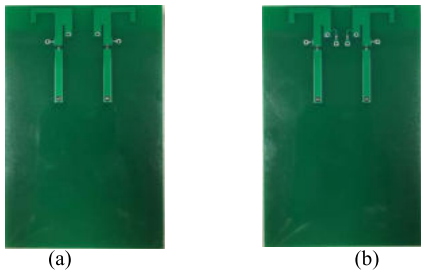

(a) (b)

Fig. 8. Prototypes of the IFA antennas in Case 1. (a) Coupled antennas. (b) Decoupled antennas.

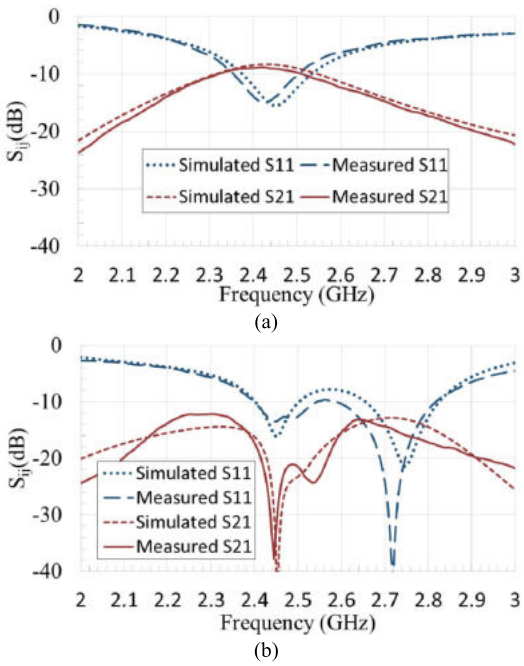

Fig. 9. Simulated and measured S-parameters in Case 1. (a) Coupled antennas. (b) Decoupled and rematched antennas.

antenna changes. As matching condition does not affect the isolation property, a rematching process will not change the decoupling property. In this case, a typical L-type matching network is adopted. The prototypes of the coupled and decoupled antennas are shown in Fig. 8. The simulated and measured S-parameters of the original coupled and matched IFA antennas and those of the decoupled and rematched IFA antennas are present in Fig. 9. It is observed that the measured isolation at the center frequency 2.45 GHz is enhanced from 8 dB to better than 35 dB, whereas the measured return loss is better than 10 dB. It is interesting to observe that the rematched antennas are with a wider bandwidth than that of the original coupled antennas. The simulated and measured results agree very well.

The simulated current distributions at 2.45 GHz for the coupled and decoupled antennas are compared in Fig. 10 with antenna 2 excited. It is observed that after adding the capacitive load, the current flowing into antenna 1 is reduced, indicating higher isolation between the two antennas.

The measured radiation patterns of the coupled and decoupled antennas are shown in Fig. 11. In the measurement,

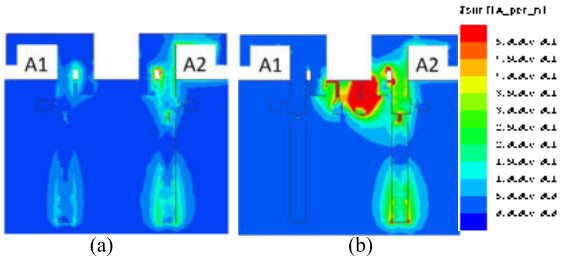

Fig. 10. Simulated current distributions when antenna 2 (A2) is excited in Case 1. (a) Coupled antennas. (b) Decoupled antennas.

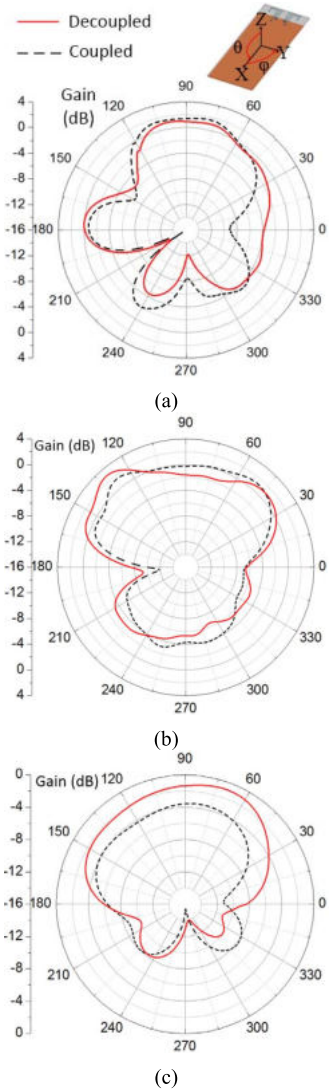

Fig. 11. Measured radiation patterns of antenna 2 in Case 1. (a) *xy* plane. (b) *xz* plane. (c) *yz* plane.

antenna 1 is terminated with a matched load and antenna 2 is excited. One direct observation is that the radiation patterns will not change too much after decoupling as compared with those of the coupled antenna. This desirable feature is understandable, since the decoupling method minimally disturbs the current distribution on radiating arms of the antennas.

It is well known that for MIMO antennas, ECC is an important figure of merit. A low ECC means low spatial correlation

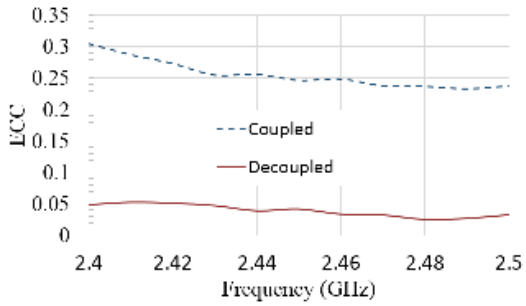

Fig. 12. Measured ECC of coupled and decoupled IFA antennas in Case 1.

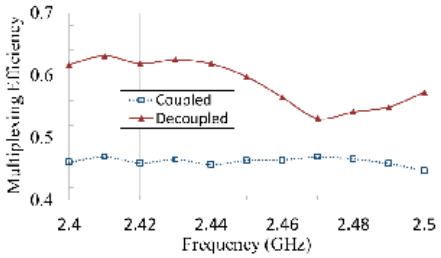

Fig. 13. Measured multiplexing efficiencies of antennas in Case 1.

between antennas. The ECCs for the coupled and decoupled IFA antennas can be calculated [26] using the measured far-field radiation patterns of two antennas. As shown in Fig. 12, a significant improvement (from 0.25 to 0.05) for ECC is achieved by using the proposed decoupling technique. Another important figure of merit for an MIMO antenna system is its multiplexing efficiency [27]. A higher multiplexing efficiency means better MIMO performance. Thus, the multiplexing efficiencies for the coupled and decoupled antennas are also calculated using the measured ECCs and total efficiencies. As compared in Fig. 13, the multiplexing efficiency of the two antennas in the case is improved from 46% to 60% after using the decoupling technique.

B. Case 2 (Two Tail-to-Tail IFAs Working in LTE Band 3)

To study the improvement on an MIMO system by using this decoupling technique in terms of the throughput in a multipath channel environment, two tail-to-tail IFA antennas working at 1.8425 GHz (LTE Band 3) with and without decoupling capacitive loads are designed and fabricated. The configuration of the antennas with the capacitive loads is shown in Fig. 14. Different from Case 1, these two antennas are deposited on a 3-D printed plastic stand. The length of the bent arm marked as l_{12} is 6 mm. Both antennas are fed using coplanar waveguide transmission lines. To test the system performance in a mobile phonelike platform, the antenna pair with and without decoupling loads are connected with a commercially available HUAWEI ME909s-821 two-port MIMO LTE module. The prototype of the whole system is shown in Fig. 15(a). The measured S-parameters for the coupled and the decoupled antennas are shown in Fig. 16. It is found that in the 10-MHz downlink bandwidth (1.8375–1.8475 GHz), the coupling is reduced from about −8 to −18 dB after decoupling and the matching conditions for both the coupled and decoupled

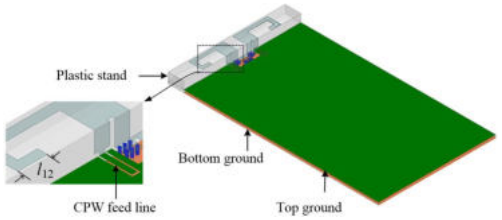

Fig. 14. Configuration of two tail-to-tail IFA antennas with capacitive loads for Case 2. The blue dots denote the short vias.

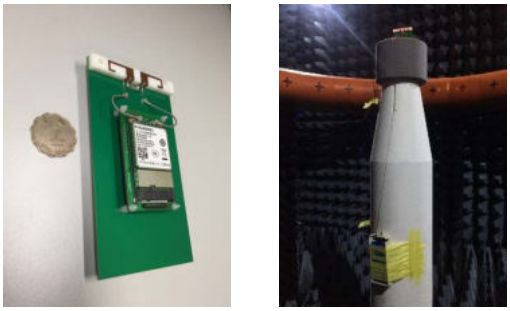

(a) (b)

Fig. 15. MIMO throughput test in Case 2. (a) DUT. (b) Multiprobe anechoic chamber.

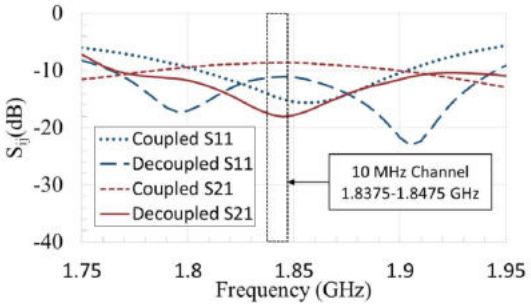

Fig. 16. Measured S-parameters for coupled and decoupled antennas in Case 2.

antennas are better than −10 dB. The measured total efficiency throughout the interested bandwidth is improved from 51% to 60% after decoupling.

Different from the single input single output scheme, a multipath channel environment must be used to measure the over-the-air (OTA) performance of an MIMO system. In this paper, two Anite FS8 eight-channel emulators are used to create the desired spatial channel model-extended Urban Microcell (UMi) and Urban Macrocell (UMa) channel environments. The emulated channel signals are created by eight dual-polarized antennas on a horizontal ring in an anechoic chamber [28]. The measurement setup is shown in Fig. 15(b). It should be noted that this measurement setup is a standard solution recommended by CTIA and 3GPP for MIMO OTA test, by which the throughput performance is the only figure of merit for MIMO test [29].

The setup for the MIMO OTA test is shown in Fig. 17. The CMW500 communication tester works as an MIMO base station sending two MIMO data stream signals. The two data streams pass through two FS8 emulators and eight

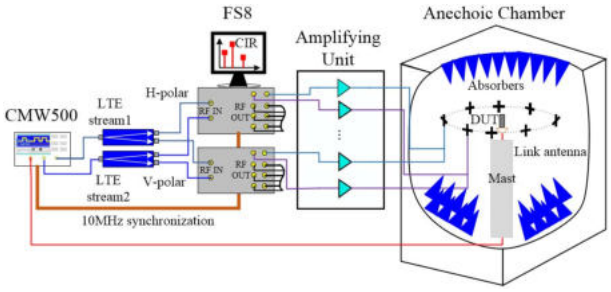

Fig. 17. Setup for MIMO OTA test.

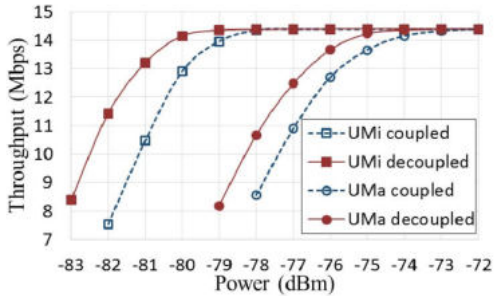

Fig. 18. Measured average throughputs versus power tested in UMi and UMa channel environments for the coupled and decoupled IFA antennas in Case 2.

dual-polarized antennas to create the specified channel environment. The channel characteristics include per-path delay, Doppler effect, the angle of departure, angle of arrival, and polarization. The device under test (DUT) will be placed on the foam mast positioned at center of the ring.

The OTA tests consist of two parts: the DUT for the coupled antennas and the DUT for the decoupled antennas. In the test, the duplex mode is frequency division duplex and the downlink channel bandwidth is 10 MHz (1837.5–1847.5 MHz). The downlink modulation is 16QAM and the maximum theoretical throughput is 14.386 Mbps.

For a given transmitting power from the base station, the OTA test is repeated with the DUT rotated every 45 degree in the horizontal plane. The average value of these eight test results will be regarded as the average throughput. The average throughputs for the coupled and decoupled cases under UMi and UMa environments are compared in Fig. 18. In the UMi environment, when the throughput drops from the peak value 14.386 to 13 Mbps (about 90% of the peak value), the required power after decoupling is reduced from −79.9 to −81.1 dBm, which means that there is 24% of power saving for achieving the same MIMO performance as compared with the coupled antennas. Similarly, the required input power after decoupling is reduced by about 0.8 dB under the UMa channel model.

C. Cases 3–8 (Other Antenna Arrangements)

As shown in Fig. 19, Cases 3–8 are also studied to justify the generality of this decoupling technique. The dimensional parameters of the IFA antennas and the stubs are listed in Table I. Following the same design procedure as that for Case 1, good isolation can be obtained for Cases 3–8. To save space, only the values of the loaded capacitors, the

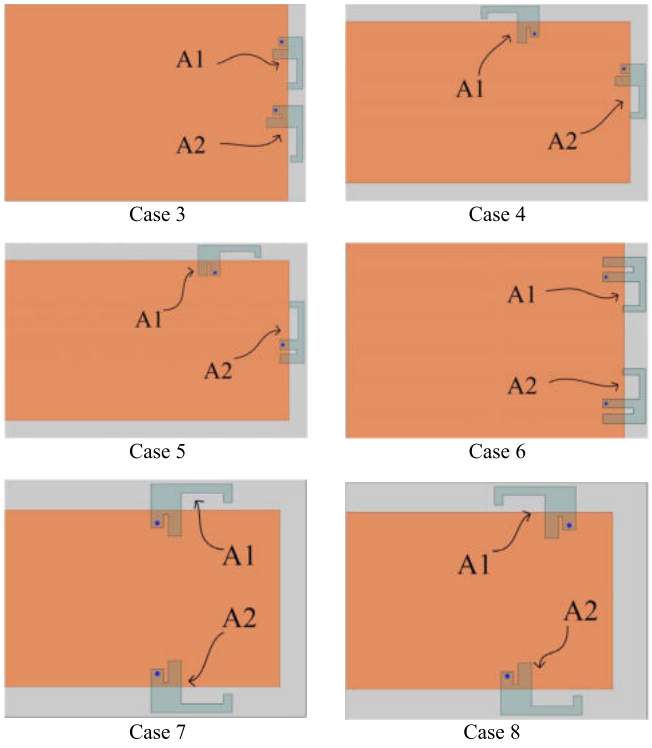

Fig. 19. Six cases of other possible arrangements for two coupled IFA antennas for Cases 3–8. The dots denote the grounding vias.

TABLE II
SUMMARY FOR CASES 3–8 (ISOLATION IN dB)

Cases	3	4	5	6	7	8
Loaded Capacitor (pF)	1	0.8	1.5	1.6	2.5	2.2
In-band Max. Isolation for Coupled Case	7.9	13	10.8	9.5	10.9	13.5
In-band Min. Isolation for Decoupled Case	14.6	23.4	23.7	22.5	17.8	21.3
Isolation @ 2.45 GHz for Coupled Case	7.5	12.8	10.5	8.8	10.6	13.2
Isolation @ 2.45 GHz for Decoupled Case	28.4	33.3	45.6	38.6	23.3	27
Matching circuit (A1)	2 nH, 1.3 pF	1.8 pF, 8 pF, 1.1 nH, 4.7 pF	1.4 pF, 8.2 pF, 1.1 nH, 4.7 pF	7.5 nH, 6.8 nH, 0.7 pF	4.7 pF, 6.8 pF, 1.3 nH	4.3 pF, 2 nH, 3.3 pF
Matching circuit (A2)	2 pF, 10 nH, 0.7 pF, 10 nH	2.2 pF, 5.6 pF, 1.5 nH, 3.9 pF	0.2 pF, 6.2 nH, 0.4 pF	7.5 nH, 6.8 nH, 0.7 pF	4.7 pF, 6.8 pF, 1.3 nH	4.3 pF, 1.8 nH, 3.3 pF

maximum (max.) isolation of the coupled antennas in the working band (2.4–2.5 GHz), the minimum (min.) isolation of the decoupled antennas in the band, the isolation at the center frequency (2.45 GHz) for the coupled and decoupled antennas and the matching circuits are summarized in Table II. In all cases, the return loss is better than 10 dB in the band of interest in both coupled and decoupled cases. It is observed that this technique can achieve good decoupling performance for all the six cases.

IV. Conclusion and Future Works

This paper proposes a self-curing decoupling technique for effectively reducing the coupling between two closely placed IFA antennas. It is called self-curing as only a capacitive load is added at an "acupoint" of each IFA antenna without requiring external "operations," such as a physical connection or a structure between two coupled IFA antennas. This nonconnection feature provides a great convenience in practical implementation. The added capacitive load occupies very little space so that it is suitable for modern wireless terminals where the circuit board is densely populated by electronic components. In addition, the size of the capacitive load is insensitive to frequency, making the decoupling technique very attractive for low-frequency band applications, such as LTE bands 12 and 13. The three-step design procedure of this technique is simple and a general design formula is given. The generality of the decoupling technique has been demonstrated by a wide range of practical scenarios with two IFAs in different arrangements. The improvement in the port isolation, total radiation efficiency, ECC, and above all the throughput justifies the effectiveness and usefulness of the proposed decoupling technique. Although the decoupling technique has been proven effective for two IFAs, it has been found by the authors that the technique can also be applied to many other types of antennas as long as an acupoint can be found. The technique can also be applied to an array antenna with more than two elements, but the network solution will be associated with higher order nonlinear equations. More research in these directions will be reported in near future.

References

[1] M. A. Jensen and J. W. Wallace, "A review of antennas and propagation for MIMO wireless communications," *IEEE Trans. Antennas Propag.*, vol. 52, no. 11, pp. 2810–2824, Nov. 2004.

[2] S. Hong *et al.*, "Applications of self-interference cancellation in 5G and beyond," *IEEE Commun. Mag.*, vol. 52, no. 2, pp. 114–121, Feb. 2014.

[3] M. Pelosi, M. B. Knudsen, and G. F. Pedersen, "Multiple antenna systems with inherently decoupled radiators," *IEEE Trans. Antennas Propag.*, vol. 60, no. 2, pp. 503–515, Feb. 2012.

[4] S. Zhang, K. Zhao, Z. Ying, and S. He, "Investigation of diagonal antenna-chassis mode in mobile terminal LTE MIMO antennas for bandwidth enhancement," *IEEE Antennas Propag. Mag.*, vol. 57, no. 2, pp. 217–228, Aug. 2015.

[5] Z. N. Chen, X. N. Low, and T. S. P. See, "Analysis and optimization of compact suspended plate MIMO antennas," *IEEE Trans. Antennas Propag.*, vol. 59, no. 1, pp. 263–270, Jan. 2011.

[6] A. Diallo, C. Luxey, P. L. Thuc, R. Staraj, and G. Kossiavas, "Study and reduction of the mutual coupling between two mobile phone PIFAs operating in the DCS1800 and UMTS bands," *IEEE Trans. Antennas Propag.*, vol. 54, no. 11, pp. 3063–3074, Nov. 2006.

[7] S.-W. Su, C.-T. Lee, and F.-S. Chang, "Printed MIMO-antenna system using neutralization-line technique for wireless USB-dongle applications," *IEEE Trans. Antennas Propag.*, vol. 60, no. 2, pp. 456–463, Feb. 2012.

[8] A. C. K. Mak, C. R. Rowell, and R. D. Murch, "Isolation enhancement between two closely packed antennas," *IEEE Trans. Antennas Propag.*, vol. 56, no. 11, pp. 3411–3419, Nov. 2008.

[9] B. K. Lau and J. B. Andersen, "Simple and efficient decoupling of compact arrays with parasitic scatterers," *IEEE Trans. Antennas Propag.*, vol. 60, no. 2, pp. 464–472, Feb. 2012.

[10] L. Zhao and K.-L. Wu, "A decoupling technique for four-element symmetric arrays with reactively loaded dummy elements," *IEEE Trans. Antennas Propag.*, vol. 62, no. 8, pp. 4416–4421, Aug. 2014.

[11] C.-Y. Chiu, C.-H. Cheng, R. D. Murch, and C. R. Rowell, "Reduction of mutual coupling between closely-packed antenna elements," *IEEE Trans. Antennas Propag.*, vol. 55, no. 6, pp. 1732–1738, Jun. 2007.

[12] S. Zhang, B. K. Lau, Y. Tan, Z. Ying, and S. He, "Mutual coupling reduction of two PIFAs with a T-shape slot impedance transformer for MIMO mobile terminals," *IEEE Trans. Antennas Propag.*, vol. 60, no. 3, pp. 1521–1531, Mar. 2012.

[13] A. A. Isaac, H. M. Al-Rizzo, A. I. Hammoodi, and H. R. Khaleel, "Mutual coupling reduction between two closely spaced inverted-F antennas," in *Proc. USNC-URSI Radio Sci. Meeting/Joint AP-S Symp.*, 2015, p. 53.

[14] F. Yang and Y. Rahmat-Samii, "Microstrip antennas integrated with electromagnetic band-gap (EBG) structures: A low mutual coupling design for array applications," *IEEE Trans. Antennas Propag.*, vol. 51, no. 10, pp. 2936–2946, Oct. 2003.

[15] L. Yang, M. Fan, F. Chen, J. She, and Z. Feng, "A novel compact electromagnetic-bandgap (EBG) structure and its applications for microwave circuits," *IEEE Trans. Microw. Theory Techn.*, vol. 53, no. 1, pp. 183–190, Jan. 2005.

[16] J. Andersen and H. Rasmussen, "Decoupling and descattering networks for antennas," *IEEE Trans. Antennas Propag.*, vol. AP-24, no. 6, pp. 841–846, Nov. 1976.

[17] J. Sui and K.-L. Wu, "A general T-stub circuit for decoupling of two dual-band antennas," *IEEE Trans. Microw. Theory Techn.*, vol. 65, no. 6, pp. 2111–2121, Jun. 2017.

[18] S. C. Chen, Y. S. Wang, and S. J. Chung, "A decoupling technique for increasing the port isolation between two strongly coupled antennas," *IEEE Trans. Antennas Propag.*, vol. 56, no. 12, pp. 3650–3658, Dec. 2008.

[19] J. Weber, C. Volmer, K. Blau, R. Stephan, and M. A. Hein, "Miniaturized antenna arrays using decoupling networks with realistic elements," *IEEE Trans. Microw. Theory Techn.*, vol. 54, no. 6, pp. 2733–2740, Jun. 2006.

[20] C. Volmer, J. Weber, R. Stephan, K. Blau, and M. A. Hein, "An eigen-analysis of compact antenna arrays and its application to port decoupling," *IEEE Trans. Antennas Propag.*, vol. 56, no. 2, pp. 360–370, Feb. 2008.

[21] J. C. Coetzee and Y. Yu, "Port decoupling for small arrays by means of an eigenmode feed network," *IEEE Trans. Antennas Propag.*, vol. 56, no. 6, pp. 1587–1593, Jun. 2008.

[22] L. K. Yeung and Y. E. Wang, "Mode-based beamforming arrays for miniaturized platforms," *IEEE Trans. Microw. Theory Techn.*, vol. 57, no. 1, pp. 45–52, Jan. 2009.

[23] L. Zhao, L. K. Yeung, and K.-L. Wu, "A coupled resonator decoupling network for two-element compact antenna arrays in mobile terminals," *IEEE Trans. Antennas Propag.*, vol. 62, no. 5, pp. 2767–2776, May 2014.

[24] L. Zhao, K.-W. Qian, and K.-L. Wu, "A cascaded coupled resonator decoupling network for mitigating interference between two radios in adjacent frequency bands," *IEEE Trans. Microw. Theory Techn.*, vol. 62, no. 11, pp. 2680–2688, Nov. 2014.

[25] K.-W. Qian, L. Zhao, and K.-L. Wu, "An LTCC coupled resonator decoupling network for two antennas," *IEEE Trans. Microw. Theory Techn.*, vol. 63, no. 10, pp. 3199–3207, Oct. 2015.

[26] S. M. Mikki and Y. M. M. Antar, "On cross correlation in antenna arrays with applications to spatial diversity and MIMO systems," *IEEE Trans. Antennas Propag.*, vol. 63, no. 4, pp. 1798–1810, Apr. 2015.

[27] Z. Ying, "Antennas in cellular phones for mobile communications," *Proc. IEEE*, vol. 100, no. 7, pp. 2286–2296, Jul. 2012.

[28] Microwave Vision Group, Paris, France. *StarMIMO*. Accessed: Jan. 18, 2018. [Online]. Available: http://www.mvg-world.com/en/products/field_product_family/antenna-measurement-2/starmimo

[29] CTIA, Washington, DC, USA. *Test Plan for* 2×2 *Downlink MIMO and Transmit Diversity Over-the-Air Performance*. Accessed: Jan. 18, 2018. [Online]. Available: https://www.ctia.org/docs/default-source/certification/ctia_mimo_ota_v1_1.pdf?sfvrsn=0

Jiangwei Sui (S'17) received the B.S. degree from the University of Science and Technology of China, Hefei, China, in 2014. He is currently pursuing the Ph.D. degree in The Chinese University of Hong Kong, Hong Kong.

His current research interests include antenna design and application for mobile communication systems.

Ke-Li Wu (M'90–SM'96–F'11) received the B.S. and M.Eng. degrees from the Nanjing University of Science and Technology, Nanjing, China, in 1982 and 1985, respectively, and the Ph.D. degree from Laval University, Quebec, QC, Canada, in 1989.

From 1989 to 1993, he was a Research Engineer with McMaster University, Hamilton, ON, Canada. He joined the Corporate Research and Development Division, Honeywell Aerospace, Cambridge, ON, Canada, in 1993, where he was a Principal Member of Technical Staff. Since 1999, he has been with The Chinese University of Hong Kong, Hong Kong, where he is currently a Professor and the Director of the Radiofrequency Radiation Research Laboratory. His current research interests include EM-based circuit domain modeling of high-speed interconnections, robot automatic tuning of microwave filters, decoupling techniques of MIMO antennas, and Internet of Things technologies.

Dr. Wu is a member of the IEEE Microwave Theory and Techniques (MTT)-8 Subcommittee. He serves as a TPC member for many prestigious international conferences. He was an Associate Editor of the IEEE Transactions on MTT from 2006 to 2009. He was a recipient of the 1998 COM DEV Achievement Award and the Asia–Pacific Microwave Conference Prize twice in 2008 and 2012, respectively.